

SUPPORT ALGORITHMS FOR X-RAY MICRO-CT CONEBEAM IMAGING

J. Gregor, T. Benson

Dept. Computer Science
University of Tennessee
Knoxville, TN 37996–3450

S.S. Gleason, M.J. Paulus

ImTek, Inc.
3200 Mynatt Ave.
Knoxville, TN 37919

1. INTRODUCTION

Small animal imaging has become an important tool in the biomedical sciences since it permits researchers to noninvasively screen animal models for mutations or pathologies as well as to monitor disease progression and response to therapy. The modality considered here is x-ray micro-CT which is useful for obtaining high-resolution volumetric anatomic images of the internal structure of an animal. In particular, we emphasize the MicroCAT™ which is a circular orbit conebeam system that originally was developed for mouse work at Oak Ridge National Laboratory [1, 2, 3] but has since then been transferred to industry for commercialization. Reconstructions are computed by means of the Feldkamp algorithm [4]. Here we present two support algorithms called XFOV and FOA which briefly can be summarized as follows.

In order to image an animal that is taller than what a given symmetric detector array configuration supports, the XFOV algorithm is used to essentially double the field of view [5]. The detector array is mechanically offset to appear as one half of a detector array that is twice as wide. To compensate for the missing projection data, we apply an interpolation and weighting scheme during reconstruction. Applied on its own, the weighting scheme can be used for fast animal screening since it allows an image volume to be reconstructed in about half the time it takes to compute a regular full reconstruction. The XFOV idea applies to circular orbit conebeam algorithms in general including iterative ones.

Only the voxels located inside the axial cylinder inscribed by the image volume need be considered during reconstruction [6]. However, the FOA algorithm [7], which is a *data-driven* preprocessing scheme, makes it possible to identify an even smaller, but still convex subset of voxels that include all those relevant to the object under study. By concentrating on this subset of voxels during reconstruction, the computational demands of the otherwise time consuming backprojection step of the Feldkamp algorithm can be greatly reduced without sacrificing the image quality. Presented here in connection with x-ray imaging, the FOA idea is general by nature and applies not only to other circular conebeam algorithms including iterative ones but also to other types of projection image reconstruction problems.

We provide experimental results based on the Shepp-Logan 3D head phantom as well as mouse data from a MicroCAT scanner. More results will be presented at the meeting.

This work was supported by the National Institutes of Health under grant number 1 R01 EB00789-01A2. The computer equipment was acquired as part of SInRG, a University of Tennessee grid infrastructure grant supported by the National Science Foundation under grant number EIA-9972889. Email correspondence to: jgregor@cs.utk.edu.

MicroCAT is a registered trademark of ImTek, Inc.

2. EXTENDED FIELD OF VIEW (XFOV)

Let $P(\Phi, Y, Z)$ represent the 2D projection at view angle Φ with (Y, Z) denoting the spatial location of a detector element. Normally, data is sampled for $0 \leq \Phi \leq 2\pi$, $|Z| \leq \delta_Z$, and $|Y| \leq \delta_Y$. But suppose that the detector array has been offset such that projection data is acquired for $-\delta_Y \leq Y \leq \delta_c$ where $0 < \delta_c$ while data for $\delta_c < Y \leq \delta_Y$ is missing. See Fig. 1a. Setting the missing projection data to zero is not a viable option as the discontinuity introduced thereby will be amplified by the filtering step of the Feldkamp algorithm to the point where the reconstructed image is distorted beyond recognition. A better approach is to recover the missing data. This can be achieved using rotational symmetry. That is,

$$P(\Phi, Y, Z) \equiv P(\pi + \Phi + 2 \tan^{-1}(Y/D'), -Y, Z)$$

where $D' = \sqrt{D^2 + Z^2}$ and D is the distance from the x-ray source to the center of the detector array. Strictly speaking, this relationship is true only for midplane data (for which $Z = 0$) but we have found it to be a reasonable *approximation* for off-midplane data (for which $Z \neq 0$). An important implication is that we can use bilinear interpolation to recover missing data from data that has been sampled. See Fig. 1b. Prior to backprojection, we multiply the filtered (acquired and recovered) projection data by a smooth weight function similar to the one proposed by Parker [8] in connection with his work on short-scan imaging, namely,

$$w(\Phi, Y, Z) = \begin{cases} 1 & -\delta_Y \leq Y \leq -\delta^* \\ \sin^2\left(\frac{\pi}{4} \frac{Y - \delta^*}{\delta^*}\right) & -\delta^* \leq Y \leq 0 \\ \cos^2\left(\frac{\pi}{4} \frac{Y + \delta^*}{\delta^*}\right) & 0 \leq Y \leq +\delta^* \\ 0 & +\delta^* \leq Y \leq +\delta_Y \end{cases}$$

where $\delta^* \ll \delta_Y$. See Fig. 1c. Following weighting, the data is backprojected as usual except that data which has been set to zero is ignored.

3. FOCUS OF ATTENTION (FOA)

The idea behind focus of attention can be described as follows. Consider shining a light at an animal from a number of different view angles. When backprojecting the resulting shadowgrams into the image space, the intersection thereof ideally forms a convex hull. Only the projection and image data that pertain to this hull need be considered for the reconstruction, reducing the amount of computation needed. The theory of support functions [9] provides the mathematical criteria for ensuring that the two spaces are consistent with one another.

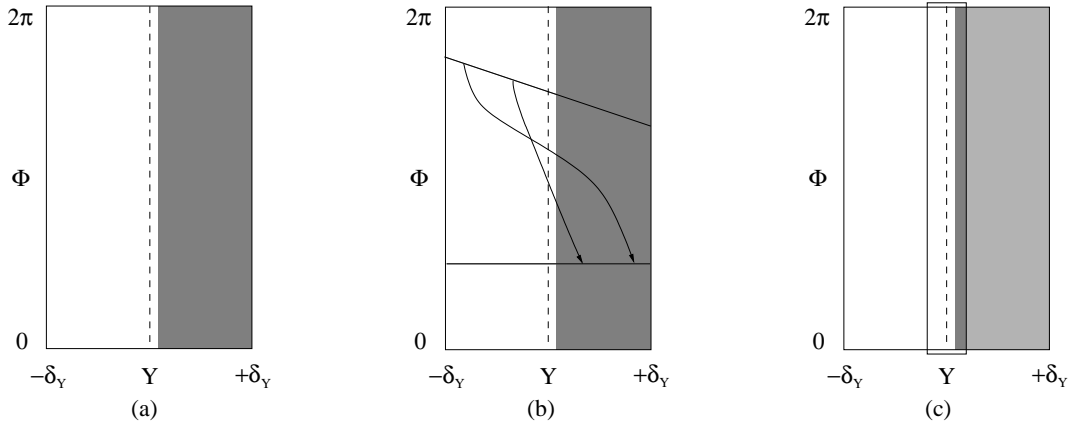


Fig. 1. Imaging using an offset detector array. (a) Projection data is only sampled for the white region for each plane (arbitrary Z). The dashed line indicates the projection center ($Y = 0$). (b) Rotational symmetry is used to obtain the missing data represented by the gray region. (c) Smooth weighting is applied to data in the outlined central window ($|Y| \leq \delta^*$). Data in the light gray region to the right is not considered during backprojection.

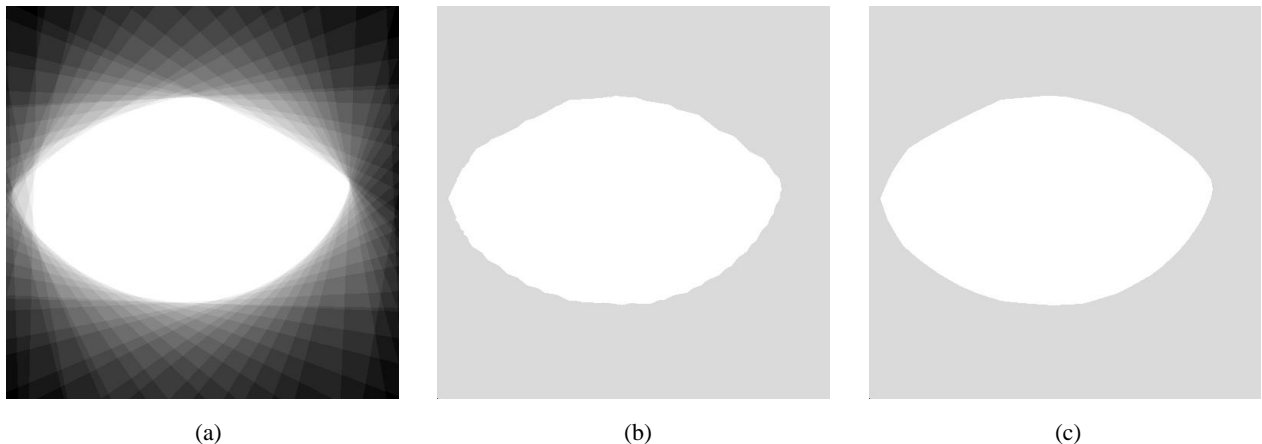


Fig. 2. Cross-section of focus of attention based reconstruction hull. (a) Example of f_B , the image that results from backprojecting the thresholded projections. (b) Point set Ω' which exhibits several concavities. (c) Derived convex hull Ω on basis of which background voxels are eliminated from the reconstruction.

As it is impractical (and unnecessary) to compute the tightest possible 3D convex hull that envelops an animal, we aim instead to compute the tightest fitting axial cylinder that has a convex cross-section. We solve the associated 2D support function estimation problem by means of the following shape-based algorithm. We first apply moving average based thresholding to determine the projection boundaries, i.e. minimum and maximum Y values, associated with a given view angle. We then create and backproject a corresponding thresholded version of the projection data. Let f_B denote the cross-section of the image volume that results after having processed all the projections. Furthermore, let $f_{\Omega'}$ be a thresholded version of f_B with Ω' denoting the set of non-zero pixels. We then compute the support vector for Ω' and use it to determine the (small number of) pixels that potentially must be added in order to obtain Ω , the desired 2D convex hull. This concludes the preprocessing step. See Fig. 2 for an illustration.

During image reconstruction, we only consider the voxels for which the (x, y) sub-coordinates lie within the Ω point set. Since

we do not alter the original projection data in any way, the values of the reconstructed image are identically the same for the Feldkamp algorithm whether we apply focus of attention or not. The integrity of interior object voxels is thus not compromised even if we were to exclude some of the peripheral object voxels. Background voxels may, of course, be assigned different values in the two cases.

Focus of attention lends itself well to iterative methods since it allows equations and unknowns to be eliminated in an algebraically consistent manner. When used for this purpose, the support vector for Ω is used to specify the subset of projection data to be considered. This support vector is identical to the one computed for Ω' and is thus readily available at no extra cost.

4. DISTRIBUTED COMPUTING

The XFOV and FOA support algorithms have been incorporated into a parallelized version of the Feldkamp algorithm [7]. With

respect to the latter, then each node is made responsible for reconstructing a particular image subvolume, the axial width of which is determined by the node's rank in the computation. The corners of the image subvolume are projected out to the detector space to determine the subset of the projection data needed locally. This data is then processed without the need for communicating with the other nodes. The cost incurred by having the same projection data be corrected and filtered on several nodes is to a great extent offset by not having the nodes exchange large projection data sets. Furthermore, the implementation is straightforward.

The LAM version of MPI is used to initialize the overall computation (including getting remote processes started and assigning rank to the nodes) as well as to implement the reduction operation needed when determining the global FOA projection boundaries for each view angle. Standard POSIX threads are used to facilitate shared-memory based multi-processor computations on each node.

5. EXPERIMENTAL RESULTS

This section serves to illustrate the quality and computational efficiency of the XFOV and FOA support algorithms. The computing environment consists of twenty-four PCs, each equipped with two 2.4GHz Pentium 4 processors and 2 Gbytes of shared-memory. The operating system is Linux. The PCs are interconnected via Gigabit ethernet.

Our first set of results are in regard to XFOV. This work is based on the Shepp-Logan 3D head phantom [6]. Data is simulated for 360 view angles. Each 256×256 ($Y \times Z$) projection is truncated to 138×256 to make the data appear as if it were obtained using an offset detector array. We use a 10 pixel wide window for the smooth weighting. The conebeam angle is 12 degrees. Figure 3 shows transaxial slice 99 of the reconstructed $256 \times 256 \times 256$ image volume together with a line attenuation plot and the results of a region-of-interest (ROI) analysis. The reconstructed slice looks almost identical to the phantom itself. The line attenuation plot shows that the reconstructed values are in close agreement with the true values; the exception being with respect to values at or near steep edges but that is typical also for a full (un-truncated) reconstruction. Other transaxial slices behave similarly. The ROI analysis, which consists of a slice-by-slice comparison of the mean, minimum, and maximum ROI values associated with the XFOV reconstruction and a full reconstruction, gives further support. The provided plot, for example, shows that the ratios of these three statistics are close to one across all slices for the dark gray background ellipse. Other ROIs exhibit similar or better behavior. The overall quality of an XFOV phantom reconstruction is thus comparable with that of a regular full reconstruction.

Our second set of results illustrates FOA used in connection with mouse data obtained with the MicroCAT (ImTek Inc., TN). Here $P_{\Phi} = -\log(I_{\Phi} - I_D)/(I_0 - I_D)$ where I_{Φ} is the photon flux recorded with an animal present, and I_0 and I_D are blank and dark current projections used for normalization purposes. We have configured this system to have a conebeam angle of approximately 18 degrees. Projections are again acquired for every 1 degree up to a full 360 degree rotation of the gantry. Each projection is down-sampled to 512×1022 . We reconstruct a $512 \times 512 \times 1022$ image volume with cubic $120 \mu\text{m}$ voxels. Higher resolution images are possible by not downsampling the projection data as was done here. Figure 4 shows transaxial slice 580. The cross-section of the reconstruction hull covers 76,487 pixels or 62 percent less than the

205,887 pixels covered by the inscribed circle normally used to define the computational region-of-interest. Compared with a regular full reconstruction we observe no differences other than for the background voxels; thus, as stated above, FOA does not compromise the internal anatomical structure revealed by the Feldkamp algorithm. Figure 4 also shows the result of reconstructing using both XFOV and FOA. The projection data was first truncated to 276×1022 to simulate the detector array being offset. The only difference between the pure FOA image and the one for which XFOV has also been applied is that the latter appears slightly more grainy due to being based on reduced count statistics. There are no visible structural differences.

We close by commenting on the computational efficiency of XFOV and FOA. See Table 1. Data handling, which includes projection loading and normalization, takes longer in both cases but the added overhead is small compared with the overall time spent on a reconstruction. The data recovery associated with XFOV takes an insignificant amount of time. Likewise, the time required to establish the convex FOA reconstruction hull is negligible (partly because the preprocessing here is based on every twelfth projection as opposed to all of them). Filtering takes the same time in all cases. Finally, XFOV and FOA reduce the otherwise time consuming backprojection computation by 45 and 60 percent, respectively, which translates into similar overall time savings. The combined time savings of XFOV and FOA are on the order of 75 percent.

6. REFERENCES

- [1] M.J. Paulus, H. Sari-Sarraf, S.S. Gleason, M. Bobrek, J.S. Hicks, D.K. Johnson, J.K. Behel, and L. Thompson, "A new x-ray computed tomography system for laboratory mouse imaging," *IEEE Trans. Nuc. Sci.*, vol. 46, pp. 558–64, 1999.
- [2] S.S. Gleason, H. Sari-Sarraf, M.J. Paulus, D.K. Johnson, S.J. Norton, and M.A. Abidi, "Reconstruction of multi-energy x-ray computed tomography images of laboratory mice," *IEEE Trans. Nuc. Sci.*, vol. 46, pp. 1081–1086, 1999.
- [3] M.J. Paulus, S.S. Gleason, S.J. Kennel, P.R. Hunsicker, and D.K. Johnson, "High resolution x-ray computed tomography: An emerging tool for small animal cancer research," *Neoplasia*, vol. 2, pp. 62–70, 2000.
- [4] L.A. Feldkamp, L.C. Davis, and J.W. Kress, "Practical conebeam algorithm," *J. Opt. Soc. Am. A*, vol. 1, pp. 612–619, 1984.
- [5] J. Gregor, S.S. Gleason, and M.J. Paulus, "Conebeam x-ray computed tomography with an offset detector array," submitted to *IEEE Intl. Conf. Image Proc. 2003*.
- [6] A.C. Kak and M. Slaney, *Principles of Computerized Tomographic Imaging*, SIAM, 2001.
- [7] J. Gregor, S.S. Gleason, M.J. Paulus, and J. Cates, "Fast Feldkamp reconstruction based on focus of attention and distributed computing," to appear in *International Journal for Imaging Systems and Technology*.
- [8] D.L. Parker, "Optimal short-scan convolution reconstruction for fanbeam CT," *Medical Physics*, vol. 9, pp. 254–257, 1982.
- [9] W.C. Karl, S.R. Kulkarni, G.C. Verghese, and A.S. Willsky, "Local tests for consistency of support hyperplane data," *J. Math. Imaging and Vision*, vol. 6, pp. 249–267, 1995.

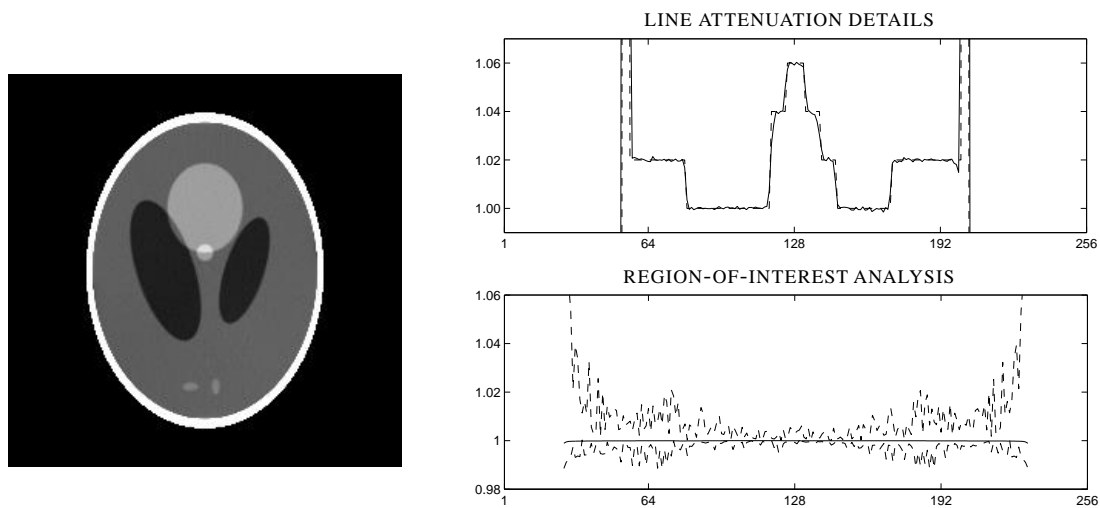


Fig. 3. Shepp-Logan XFOV example. Reconstructed transaxial slice 99 (left) with graylevels compressed from $[0.00; 2.00]$ to $[0.95; 1.05]$ for improved contrast. Attenuation across a line through the slice (top, right): solid lines are reconstruction results while dashed lines indicate ground truth. Region-of-interest analysis for large gray background ellipse (bottom, right): ratios of mean (middle solid line), minimum (lower dashed line) and maximum (upper dashed line) values for an XFOV versus a regular full reconstruction.

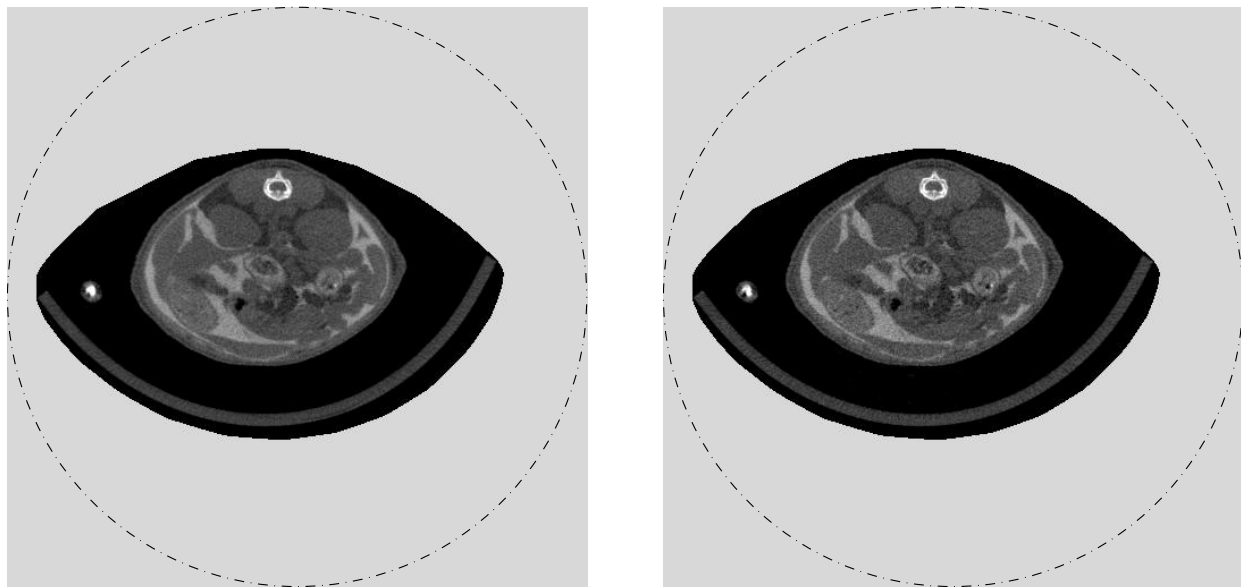


Fig. 4. Mouse example. Reconstructed transaxial slice 580 obtained using FOA (left) and XFOV+FOA (right). Graylevels are compressed for improved contrast. The light gray regions surrounding the mouse data indicate voxels not considered during reconstruction. The dashed line indicates the inscribed circle normally used to define the computational region-of-interest. The mouse received an intraperitoneal injection of a water-soluble iodinated contrast agent prior to being scanned.

	Data handling	Data recovery	Convex hull	Filtering	Backprojection
Regular recon.	0.15	–	–	0.08	8.14
w/XFOV	0.23	0.11	–	0.08	4.50
w/FOA	0.16	–	0.02	0.08	3.14
w/XFOV+FOA	0.24	0.11	0.02	0.08	1.73

Table 1. Average per-node timing results (in minutes) for volumetric mouse reconstructions. Data handling includes projection loading and normalization. Data recovery and convex hull computations refer to XFOV and FOA preprocessing, respectively. Filtering and backprojection make up the Feldkamp computations.